ROYAL SOCIETY
OF CHEMISTRY

EDGE ARTICLE

Check for updates

Unraveling the positive effect of twisted helicene structure on narrowband electroluminescence

Cheng-Zhuo Du,†[a] Minqiang Mai,†[b] Pei-Han Gao,[a] Yi-Chao Zhao,[a] Xiang-Yu Gao,[a] Dongdong Zhang,*[b] Lian Duan, [ID] *[b] Chunming Cui [ID] [a] and Xiao-Ye Wang [ID] *[ac]

Multi-resonance (MR) materials based on 1,4-BN-heteroarenes have attracted extensive attention in recent years for their narrowband electroluminescence. Extending the π-conjugation of MR skeletons is a widely adopted strategy to regulate their emission colors, but it inevitably induces structural distortion and undesirable vibronic couplings, thus broadening the emission bandwidth. Herein, we design and synthesize new MR emitters *via* π-extension of a classic MR backbone (CzBN) and disclose how the twisted structure plays a positive role in reducing the emission bandwidth. Specifically, π-extension of CzBN to form a [5]helicene substructure (BN-5H) induces serious vibrations, while further extending the helicene moiety to build a [7]helicene substructure (BN-7H) suppresses undesirable vibrations by locking the conformation. As a consequence, BN-7H achieves a smaller full-width at half-maximum (FWHM) of 28 nm compared with BN-5H (33 nm) in organic light-emitting diodes and longer device lifetime. These results overturn the traditional cognition of the detrimental effect of highly twisted structures on narrowband emission and offer a new design concept for the future development of narrowband electroluminescence materials.

Introduction

Narrowband organic light-emitting diodes (OLEDs) are highly desirable for the future ultrahigh-definition displays with a wide color gamut.[1] In 2016, Hatakeyama *et al.* developed a new type of multi-resonance (MR) materials by employing the opposite resonance effect of boron and nitrogen to separate the frontier molecular orbitals on different atoms,[2] leading to narrowband emission. As a representative MR skeleton, CzBN has been widely studied due to its merits of easy functionalization and excellent device performance (Fig. 1).[3–11] Extending the π-conjugation of CzBN by fusing benzene rings has been proven as a viable strategy to tune the emission color. Particularly, a number of green emitters for narrowband OLEDs have been developed in recent years based on this strategy.[12–17] However, upon extension of the π-skeleton, the steric repulsion between the spatially close benzene rings inevitably intensifies structural distortion and leads to additional vibrations, thus broadening

the emission spectra, with full-widths at half-maximum (FWHMs) mostly exceeding 30 nm. Therefore, it is generally believed that enhancing the planarity of the MR skeleton is beneficial to achieving narrowband emission.[3,18–21]

Herein, we design and synthesize new MR emitters (BN-5H and BN-7H) *via* π-extension of CzBN and disclose the positive effect of the twisted structure on narrowband electroluminescence (Fig. 1). BN-5H, comprising a [5]helicene substructure, exhibits serious structural vibrations similar to those of previously reported CzBN derivatives.[13,17] In contrast, BN-7H, with an elongated [7]helicene moiety, significantly suppresses the undesirable vibrations by locking the conformation. Moreover, the highly twisted structure of BN-7H also suppresses solid-state emission quenching and spectral broadening, which are common problems for planar MR emitters.[22–24] Therefore, BN-7H achieves a smaller FWHM of only 28 nm (0.12 eV) compared with BN-5H (33 nm/0.16 eV) in OLEDs. The FWHM of BN-7H is the smallest among the reported green MR materials based on benzene-fused CzBN derivatives. Besides, a high maximum external quantum efficiency (EQE_max) of 26.2% and long operation lifetime of 560.1 h at 1000 cd m^{-2} are obtained for BN-7H-based devices. These results shed new light on the positive role of twisted helicene structures for narrowband electroluminescence materials.

Results and discussion

The synthetic routes to BN-5H and BN-7H are shown in Scheme 1. Although aza[5]helicene (5H) is commercially available, the

[a]State Key Laboratory of Elemento-Organic Chemistry, Frontiers Science Center for New Organic Matter, Haihe Laboratory of Sustainable Chemical Transformations, Academy for Advanced Interdisciplinary Studies, College of Chemistry, Nankai University, Tianjin, 300071, China. E-mail: xiaoye.wang@nankai.edu.cn; Web: http://wang.nankai.edu.cn

[b]Key Lab of Organic Optoelectronics and Molecular Engineering of Ministry of Education, Department of Chemistry, Tsinghua University, Beijing, 100084, China. E-mail: ddzhang@mail.tsinghua.edu.cn; duanl@mail.tsinghua.edu.cn

[c]Beijing National Laboratory for Molecular Sciences, Beijing, 100190, China
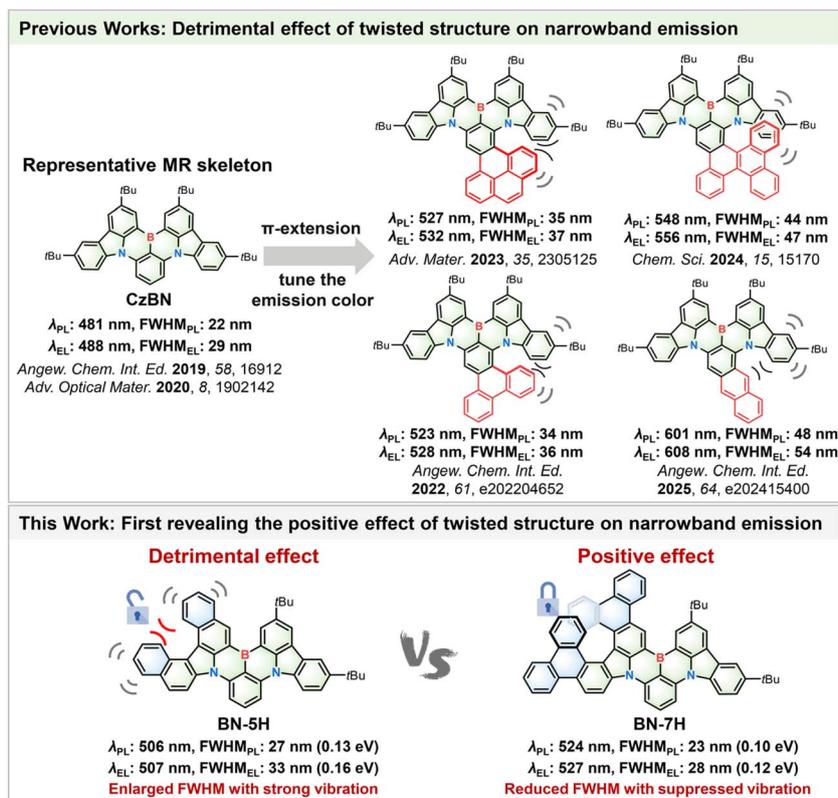
† These authors contributed equally.

Fig. 1 The representative MR emitter CzBN and molecular design of BN-5H and BN-7H. λ_{PL} and λ_{EL}: the peak wavelengths of the photoluminescence (PL) and electroluminescence (EL) spectra, respectively. $FWHM_{PL}$ and $FWHM_{EL}$: full-widths at half-maximum (FWHMs) of the PL and EL spectra, respectively.

higher homologue aza[7]helicene requires complicated synthesis in eight steps.[25,26] We thus adopted dibenzoaza[7]helicene (7H), which can be easily synthesized in only two steps,[27] as a building block to access the target compound BN-7H. First, precursors 5H-Br and 7H-Br were synthesized through aromatic nucleophilic substitution of compound 1 with 5H and 7H, respectively. Then, BN-5H and BN-7H were obtained via one-pot borylation in yields of 36% and 51%, respectively (for details, see the SI). Thermogravimetric analysis (TGA) indicates that BN-5H and BN-7H possess excellent thermal stability with high decomposition temperatures (T_d) of 503 °C for BN-5H and 547 °C for BN-7H

(Fig. S1), assuring the feasibility of thermal sublimation for further purification and OLED fabrications. According to the cyclic voltammetry (CV) characterizations (Fig. S2 and Table S1), the highest occupied molecular orbital (HOMO) and lowest unoccupied molecular orbital (LUMO) energy levels are calculated to be −5.42/−2.97 eV for BN-5H and −5.40/−3.01 eV for BN-7H, respectively. Therefore, the corresponding electrochemical energy gaps (E_{gap}) are deduced as 2.45 eV and 2.39 eV for BN-5H and BN-7H, respectively.

To further understand the geometric and electronic properties of BN-5H and BN-7H, time-dependent density functional
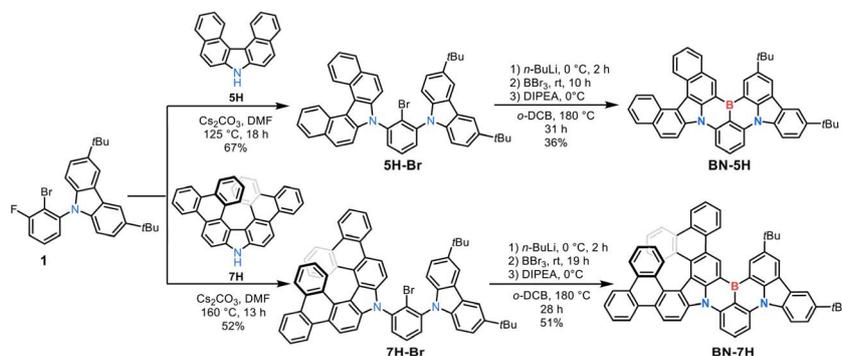
Scheme 1 Synthetic routes to BN-5H and BN-7H. DMF: *N,N*-dimethylformamide; DIPEA: *N,N*-diisopropylethylamine; and *o*-DCB: 1,2-dichlorobenzene.

theory (TD-DFT) calculations were performed at the B3LYP/6-311G(d,p) level. Compared with BN-5H, BN-7H features a more twisted geometry, with a dihedral angle of 44.98° between the terminal benzene rings (Fig. S13). According to the optimized geometries, the root-mean-square deviation (RMSD) values between S_0 and S_1 states were calculated to be 0.107 Å and 0.091 Å for BN-5H and BN-7H, respectively (Fig. 2A). Moreover, the total reorganization energy (λ) of BN-7H (0.125 eV) is much smaller than that of BN-5H (0.380 eV). These results indicate that the structural relaxation is effectively suppressed by further extending the helicene moiety.

To gain a deeper understanding of the vibronic coupling of BN-5H and BN-7H, the Huang-Rhys (HR) factors and λ at different vibrational modes were calculated using the Molecular Materials Property Prediction Package (MOMAP) software (Fig. 2B).[28] For BN-5H, two large HR factors of 0.95 and 0.48 are observed in the low-frequency region, which are related to the out-of-plane twisting vibrations of the MR framework and the peripheral *tert*-butyl groups (Modes 1 and 33). Moreover, the high-frequency stretching vibrational modes 153 (1254.78 cm^{-1}) and 204 (1589.96 cm^{-1}) of BN-5H contribute significantly to λ (Fig. S14), which may induce obvious spectral broadening. In contrast, BN-7H displays significantly suppressed out-of-plane skeleton twisting vibrations (Modes 2, 7, 9) with smaller HR factors (0.54, 0.47, 0.40) in the region 14.52–50.94 cm^{-1}. The suppressed vibrations of BN-7H can be attributed to the strong intramolecular noncovalent

interactions from the terminal benzene rings, which can be visualized by the reduced density gradient (RDG) analysis (Fig. 2D).[29] Besides, compared with BN-5H, the high-frequency stretching vibrations of BN-7H are almost negligible (Fig. S15). These results reveal the feasibility of introducing highly twisted structure to restrain common vibrations of MR emitters.

The photophysical properties of BN-5H and BN-7H were further studied in toluene solutions (1×10^{-5} M) (Fig. 3A and B), and the detailed data are summarized in Table 1. BN-5H and BN-7H exhibit strong absorption bands peaking at 488 nm and 508 nm, with molar extinction coefficients (ε) of 47 830 M^{-1} cm^{-1} and 56 320 M^{-1} cm^{-1}, respectively. The fluorescence maximum of BN-7H (524 nm) shows an obvious red-shift of 18 nm compared with that of BN-5H (506 nm) due to the π-extension. Benefiting from the suppressed vibrations by locking the conformation, BN-7H achieves a smaller FWHM value of only 23 nm (0.10 eV) in toluene than BN-5H (27 nm/0.13 eV). The Commission Internationale de L'Eclairage (CIE) coordinate of BN-7H is (0.22, 0.72), meeting the green color requirement of (0.21, 0.71) stipulated by the National Television System Committee (NTSC). Moreover, BN-7H exhibits a higher photoluminescence quantum yield (PLQY) of 95% than BN-5H (86%) due to the suppression of undesirable vibrations.

The transient photoluminescence spectra were next examined, and no obvious delayed components were observed in degassed solutions (Fig. S5), implying that these two emitters
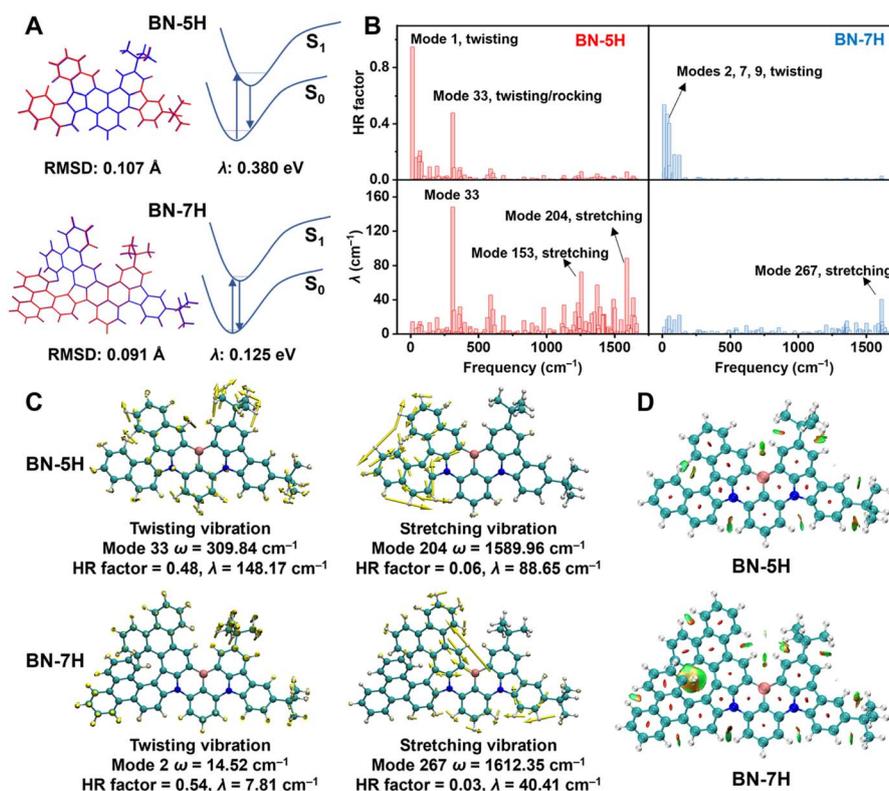

Fig. 2 Theoretical calculation results for BN-5H and BN-7H. (A) The overlap diagrams of optimized S_0 (blue) and S_1 (red) geometries and reorganization energies (λ) of BN-5H and BN-7H. (B) Plots of the Huang-Rhys (HR) factor and λ versus frequency for BN-5H and BN-7H. (C) The representative vibrational modes of BN-5H and BN-7H. (D) The reduced density gradient (RDG) isosurfaces of BN-5H and BN-7H.
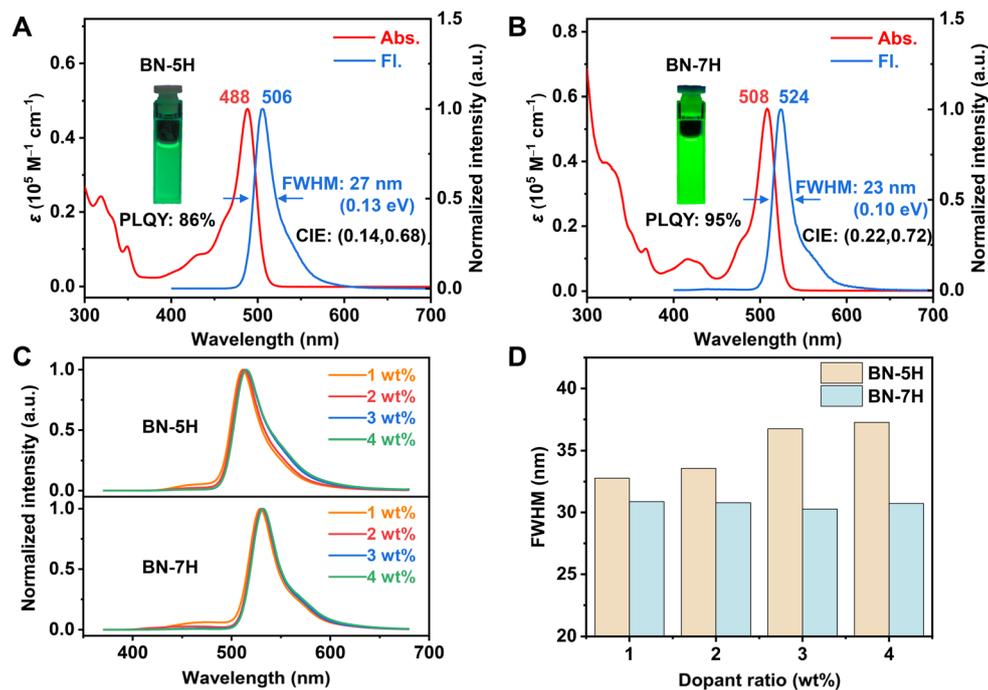
Fig. 3 Photophysical properties of BN-5H and BN-7H. UV-vis absorption (red line) and fluorescence (blue line) spectra of (A) BN-5H and (B) BN-7H in toluene solution (1×10^{-5} M) at 298 K. Insets: photographs taken under 365 nm light. (C) Normalized fluorescence spectra of BN-5H and BN-7H doped in DMIC-TRZ films with different dopant concentrations. DMIC-TRZ: 1,3-dihydro-1,1-dimethyl-3-(3-(4,6-diphenyl-1,3,5-triazin-2-yl)phenyl)indeno[2,1-b]carbazole. (D) FWHMs of the doped films for BN-5H and BN-7H with different dopant concentrations.

are fluorescence materials without thermally activated delayed fluorescence (TADF) characteristics, which may be associated with the large singlet-triplet energy gaps (ΔE_{ST}) of 0.50 eV for BN-5H and 0.29 eV for BN-7H (Fig. S3).[30–33] The reduction of ΔE_{ST} of BN-7H is further investigated by the hole–electron analysis (Fig. S12). The fluorescence lifetimes (τ) were determined to be 5.3 ns and 4.0 ns for BN-5H and BN-7H, respectively, and the corresponding radiative decay rates (k_r) and nonradiative decay rates (k_{nr}) of BN-5H and BN-7H were calculated and are summarized in Table 1. BN-7H displays a faster radiative decay process with k_r of 2.4×10^8 s^{-1} and a significantly suppressed k_{nr} of only 1.3×10^7 s^{-1}, while BN-5H suffers from a more serious energy loss with k_{nr} of 2.6×10^7 s^{-1}. This difference indicates that the more twisted structure of BN-7H can lock the flexible conformation and suppress undesirable vibrations to reduce nonradiative energy dissipation.

The emission properties of the two compounds in solid state were then investigated (Fig. 3C), and 1,3-dihydro-1,1-dimethyl-3-(3-(4,6-diphenyl-1,3,5-triazin-2-yl)phenyl)indeno[2,1-b]carbazole (DMIC-TRZ) was chosen as the wide-energy-gap host.[34] As the dopant concentration increases, the emission spectra of BN-5H doped films are significantly broadened with FWHM values increasing from 33 nm to 37 nm, while the FWHMs of BN-7H-doped films are basically unchanged (FWHM: 31 nm) (Fig. 3D). Moreover, the concentration-dependent emission quenching of BN-7H is also efficiently suppressed compared with BN-5H (Table S2). These results demonstrate the beneficial effect of highly twisted structures beyond vibrational suppression at the molecular level.

Considering that BN-5H and BN-7H are fluorescence emitters, TADF-sensitized OLEDs were fabricated to evaluate the electroluminescent (EL) properties. The corresponding energy

Table 1 Photophysical, electrochemical, and thermal properties of BN-5H and BN-7H

Compound	λ_{abs}^{a} (nm)	λ_{PL}^{a} (nm)	FWHM[b] (nm/eV)	ΔE_{ST}^{c} (eV)	HOMO/LUMO[d] (eV)	E_g^{CV} (eV)	PLQY[e] (%)	τ^{f} (ns)	k_r^{g} (10^8 s^{-1})	k_{nr}^{g} (10^7 s^{-1})	T_d/T_g^{h} (°C)	CIE $(x, y)^{i}$
BN-5H	488	506	27/0.13	0.50	−5.42/−2.97	2.45	86	5.3	1.6	2.6	503/-	(0.14, 0.68)
BN-7H	508	524	23/0.10	0.29	−5.40/−3.01	2.39	95	4.0	2.4	1.3	547/258	(0.22, 0.72)

[a] Maximum wavelength of UV-vis absorption and fluorescence spectra in toluene solution (1×10^{-5} M) at 298 K. [b] FWHMs of the fluorescence spectra. [c] Obtained from the peak of the fluorescence and phosphorescence spectra in toluene solution at 77 K. [d] Obtained from the onset potentials of the first oxidative and reductive waves of CV curves, respectively. [e] Absolute photoluminescence quantum yield measured in oxygen-free toluene solution. [f] Fluorescence lifetime. [g] Radiative decay rate constant and non-radiative decay rate constant. [h] Decomposition temperature (T_d) and glass transition temperature (T_g). [i] Commission Internationale de L'Eclairage (CIE) coordinates in the CIE 1931 chromaticity diagram.
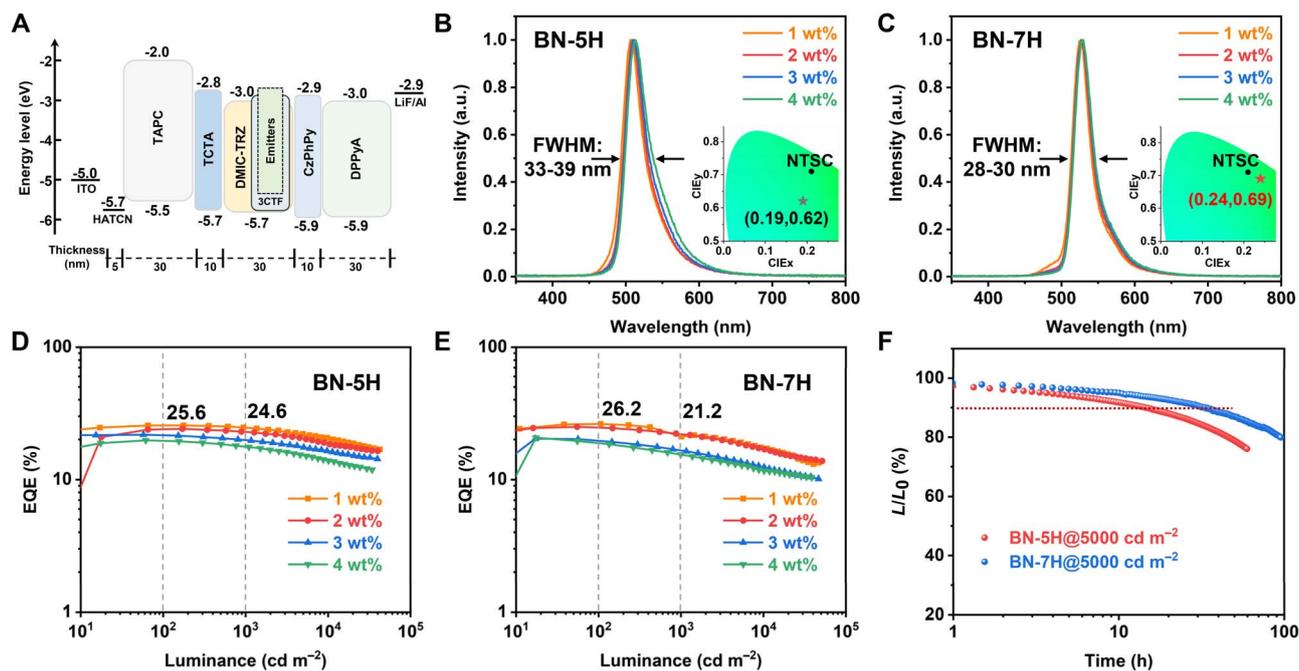
Fig. 4 EL performances of the TADF-sensitized OLED devices. (A) Device structure and the energy level diagram. (B), (C) Normalized electroluminescence spectra of BN-5H and BN-7H. Inset: CIE coordinates of the devices in CIE 1931 chromaticity diagram. The black circle is the NTSC green standard. (D), (E) EQE versus luminance characteristics of BN-5H and BN-7H. The dashed lines and values show the EQE at 100 cd m^{-2} and 1000 cd m^{-2}. (F) Lifetime data of the devices measured at an initial luminance of 5000 cd m^{-2}. The dashed line represents the lifetime to 90% of the initial luminance.

level scheme and chemical structures of the materials used are depicted in Fig. 4A and S17. Particularly, 2,4,6-tris(2-(3,6-di-*tert*-butyl-9*H*-carbazol-9-yl)-5-(trifluoromethyl)phenyl)-1,3,5-triazine (3CTF) was chosen as the TADF sensitizer because of its small molecular dipole moment, substantial spectral overlap with these emitters, and high reverse intersystem crossing rate of 2.57×10^6 s^{-1} (Fig. S18).[35] The EL characteristics are summarized in Table 2. Obviously, the devices based on BN-5H show lower tolerance to the dopant concentration, and the FWHM increases significantly with higher dopant concentrations (Fig. 4B). By contrast, the BN-7H-based devices display nearly unchanged emission peaks and FWHMs with increased dopant concentrations, and pure green emissions peaking at 527–529 nm with small FWHMs of only 28–30 nm (0.12–0.13 eV) were recorded (Fig. 4C). Such a result is one of the smallest

FWHMs among the reported sensitized green OLEDs (Table S5).[3,36–43] Besides, the CIE coordinates of BN-7H devices reach (0.24, 0.69), which is very close to the pure green requirement of the NTSC standard. Moreover, BN-7H shows outstanding device performance with EQE$_{max}$, current efficiency (CE), and power efficiency (PE) of 26.2%, 102.3 cd A^{-1}, and 106.5 lm W^{-1}, respectively (Fig. 4E). Meanwhile, the efficiency roll-off is especially low with the EQE remaining 21.2% at 1000 cd m^{-2}.

We further evaluated the operational stabilities of these devices under an initial luminance (L_0) of 5000 cd m^{-2} (Fig. 4F). The LT_{90} (lifetime to 90% of the initial luminance) of 14.5 and 33.5 h were recorded for BN-5H and BN-7H, respectively. By adopting a degradation acceleration factor (n) of 1.75,[44] the LT_{90} at 1000 cd m^{-2} can be extrapolated as 242.4 h for BN-5H and 560.1 h for BN-7H, respectively. The device lifetime of BN-7H is

Table 2 Summary of the OLED performances based on BN-5H and BN-7H

Emitter	Dopant concentration (wt%)	λ_{EL}[a] (nm)	FWHM[b] (nm/eV)	V_{on}[c] (V)	L_{max}[d] (cd m^{-2})	CE$_{max}$[e] (cd A^{-1})	PE$_{max}$[f] (lm W^{-1})	EQE[g] (%)	CIE (x, y)[h]
BN-5H	1	507	34/0.16	2.6	42 450	77.1	78.2	25.6/25.6/24.6	(0.19,0.62)
	2	509	33/0.16	2.6	40 090	76.6	74.8	24.1/24.0/22.9	(0.19,0.65)
	3	511	35/0.17	2.7	39 750	71.8	73.9	21.8/21.6/19.8	(0.20,0.66)
	4	513	39/0.18	2.7	34 360	67.7	67.0	19.7/19.3/17.6	(0.23,0.67)
BN-7H	1	527	28/0.12	2.6	47 370	102.3	106.5	26.2/26.2/21.2	(0.24,0.69)
	2	527	28/0.12	2.6	51 720	99.8	110.8	25.0/24.6/22.0	(0.25,0.69)
	3	527	29/0.13	2.6	46 890	81.0	90.9	20.3/19.7/16.6	(0.26,0.69)
	4	529	30/0.13	2.6	38 610	82.0	92.0	20.7/18.8/15.4	(0.27,0.69)

[a] The maximum EL wavelength. [b] FWHM of the EL spectrum. [c] Turn-on voltage at 1 cd m^{-2}. [d] Maximum luminance. [e] Maximum CE. [f] Maximum PE. [g] Maximum EQE, and values at 100 cd m^{-2} and 1000 cd m^{-2}. [h] CIE coordinates of the devices in the CIE 1931 chromaticity diagram.

more than twice that of BN-5H, indicating the advantages of the highly twisted structure in improving device stability.

Furthermore, it is noteworthy that BN-7H is chiral, with higher configurational stability than BN-5H due to the spatial overlapping between the terminal benzene rings (Fig. S26). Therefore, the *P* and *M* enantiomers of BN-7H were successfully separated by chiral high-performance liquid chromatography (HPLC) (Fig. S22). BN-7H exhibits circular dichroism (CD) responses with the largest absolute absorption dissymmetry factors ($|g_{abs}|$) of 0.009 at 379 nm (Fig. S24), as well as circularly polarized luminescence (CPL) with the luminescence dissymmetry factors ($|g_{lum}|$) of 0.7×10^{-3} at 524 nm and CPL brightness (B_{CPL}) of 19.0 M^{-1} cm^{-1} (Fig. S25), which are comparable to most of the reported circularly polarized MR materials (Table S6).[45–49] However, due to the limited solubility hindering the large-scale chiral separation, the EL properties of BN-7H enantiomers were not studied. Further optimizing the molecular structures and chiral separation conditions can provide promising materials for circularly polarized OLEDs with narrowband emissions in the future.[14,50–54]

Conclusions

In summary, we have designed and synthesized two new MR emitters (BN-5H and BN-7H) *via* π-extension on one carbazole moiety of the classic MR backbone CzBN and disclosed the positive role of the twisted structure in achieving narrowband OLEDs. BN-5H with a [5]helicene substructure suffers from serious structural vibrations, which is similar to other reported twisted MR emitters. In sharp contrast, BN-7H, with a [7]helicene moiety, significantly suppresses the undesirable vibrations by locking the conformation. Furthermore, the twisted structure of BN-7H also more effectively suppresses solid-state spectral broadening and fluorescence quenching compared with BN-5H. As a result, BN-7H achieves a smaller FWHM of only 28 nm (0.12 eV) compared with BN-5H (33 nm/0.16 eV) in OLEDs. Additionally, the highly twisted skeleton endows BN-7H with a high EQE_{max} of 26.2% and long device lifetime of 560.1 h at 1000 cd m^{-2}. This work has overturned the traditional cognition of the detrimental effect of twisted structure on narrowband emission and opened up a new avenue to the development of narrowband electroluminescence materials.

Author contributions

Xiao-Ye Wang, Lian Duan, Dongdong Zhang and Chunming Cui conceived the project. Cheng-Zhuo Du, Pei-Han Gao, and Yi-Chao Zhao performed the synthesis and characterization of all materials. Minqiang Mai performed the photophysical measurements of the doped films and fabricated the devices. Xiang-Yu Gao characterized the chiroptical properties. Cheng-Zhuo Du performed the theoretical calculations. Xiao-Ye Wang and Cheng-Zhuo Du wrote the original draft. All authors discussed the progress of the research and commented on the manuscript.

Conflicts of interest

There are no conflicts of interest to declare.

Data availability

The data supporting this article have been included as part of the supplementary information (SI). Supplementary information: experimental details, synthetic procedures, characterization data, NMR spectra, theoretical calculations and electroluminescence data. See DOI: https://doi.org/10.1039/d5sc08405a.

Acknowledgements

Notes and references

1 M. Sugawara, S. Y. Choi and D. Wood, *IEEE Signal Process. Mag.*, 2014, **31**, 170–174.

2 T. Hatakeyama, K. Shiren, K. Nakajima, S. Nomura, S. Nakatsuka, K. Kinoshita, J. Ni, Y. Ono and T. Ikuta, *Adv. Mater.*, 2016, **28**, 2777–2781.

3 J. Liu, Y. Zhu, T. Tsuboi, C. Deng, W. Lou, D. Wang, T. Liu and Q. Zhang, *Nat. Commun.*, 2022, **13**, 4876.

4 L. Xing, J. Wang, W.-C. Chen, B. Liu, G. Chen, X. Wang, J.-H. Tan, S. S. Chen, J.-X. Chen, S. Ji, Z. Zhao, M.-C. Tang and Y. Huo, *Nat. Commun.*, 2024, **15**, 6175.

5 Y. Pu, Q. Jin, Y. Zhang, C. Li, L. Duan and Y. Wang, *Nat. Commun.*, 2025, **16**, 332.

6 S. Madayanad Suresh, D. Hall, D. Beljonne, Y. Olivier and E. Zysman-Colman, *Adv. Funct. Mater.*, 2020, **30**, 1908677.

7 Y. Xu, Q. Wang, X. Cai, C. Li, S. Jiang and Y. Wang, *Angew. Chem., Int. Ed.*, 2023, **62**, e202312451.

8 M. Mamada, M. Hayakawa, J. Ochi and T. Hatakeyama, *Chem. Soc. Rev.*, 2024, **53**, 1624–1692.

9 J. Kang, D. J. Shin and J. Y. Lee, *Adv. Opt. Mater.*, 2025, **13**, 2402653.

10 Y. Zhang, C.-Z. Du, J.-K. Li and X.-Y. Wang, *Chin. J. Org. Chem.*, 2023, **43**, 1645–1690.

11 Y.-H. He, J.-Y. Liu, Z. Zhang, G.-W. Chen, Y.-C. Wang, G. Yuan, F.-M. Xie, J.-X. Tang and Y.-Q. Li, *Matter*, 2025, **8**, 102188.

12 Y. Zhang, D. Zhang, J. Wei, X. Hong, Y. Lu, D. Hu, G. Li, Z. Liu, Y. Chen and L. Duan, *Angew. Chem., Int. Ed.*, 2020, **59**, 17499–17503.

13 Y. Xu, Q. Wang, J. Wei, X. Peng, J. Xue, Z. Wang, S. J. Su and Y. Wang, *Angew. Chem., Int. Ed.*, 2022, **61**, e202204652.

14 T. Huang, L. Yuan, X. Lu, Y. Qu, C. Qu, Y. Xu, Y.-X. Zheng and Y. Wang, *Chem. Sci.*, 2024, **15**, 15170–15177.

15 Q. Wang, L. Yuan, C. Qu, T. Huang, X. Song, Y. Xu, Y.-X. Zheng and Y. Wang, *Adv. Mater.*, 2023, **35**, 2305125.

16 Q. Wang, Y. Xu, T. Huang, Y. Qu, J. Xue, B. Liang and Y. Wang, *Angew. Chem., Int. Ed.*, 2023, **62**, e202301930.

17 H. Chen, M. Du, C. Qu, Q. Jin, Z. Tao, R. Ji, G. Zhao, T. Zhou, Y. Lou, Y. Sun, W. Jiang, L. Duan and Y. Zhang, *Angew. Chem., Int. Ed.*, 2025, **64**, e202415400.

18 S. Jiang, Y. Yu, D. Li, Z. Chen, Y. He, M. Li, G. X. Yang, W. Qiu, Z. Yang, Y. Gan, J. Lin, Y. Ma and S. J. Su, *Angew. Chem., Int. Ed.*, 2023, **62**, e202218892.

19 G. Meng, J. Zhou, T. Huang, H. Dai, X. Li, X. Jia, L. Wang, D. Zhang and L. Duan, *Angew. Chem., Int. Ed.*, 2023, **62**, e202309923.

20 X. Wang, L. Wang, G. Meng, X. Zeng, D. Zhang and L. Duan, *Sci. Adv.*, 2023, **9**, eadh1434.

21 X. Huang, J. Liu, Y. Xu, G. Chen, M. Huang, M. Yu, X. Lv, X. Yin, Y. Zou, J. Miao, X. Cao and C. Yang, *Natl. Sci. Rev.*, 2024, **11**, nwae115.

22 P. Jiang, J. Miao, X. Cao, H. Xia, K. Pan, T. Hua, X. Lv, Z. Huang, Y. Zou and C. Yang, *Adv. Mater.*, 2022, **34**, 2106954.

23 Y. K. Qu, D. Y. Zhou, F. C. Kong, Q. Zheng, X. Tang, Y. H. Zhu, C. C. Huang, Z. Q. Feng, J. Fan, C. Adachi, L. S. Liao and Z. Q. Jiang, *Angew. Chem., Int. Ed.*, 2022, **61**, e202201886.

24 Y. Zhang, J. Wei, D. Zhang, C. Yin, G. Li, Z. Liu, X. Jia, J. Qiao and L. Duan, *Angew. Chem., Int. Ed.*, 2022, **61**, e202113206.

25 K. Uematsu, K. Noguchi and K. Nakano, *Phys. Chem. Chem. Phys.*, 2018, **20**, 3286–3295.

26 B. M. Gross and M. Oestreich, *Synthesis*, 2021, **53**, 2512–2516.

27 C. Maeda, K. Nagahata, T. Shirakawa and T. Ema, *Angew. Chem., Int. Ed.*, 2020, **59**, 7813–7817.

28 Y. Niu, W. Li, Q. Peng, H. Geng, Y. Yi, L. Wang, G. Nan, D. Wang and Z. Shuai, *Mol. Phys.*, 2018, **116**, 1078–1090.

29 E. R. Johnson, S. Keinan, P. Mori-Sánchez, J. Contreras-García, A. J. Cohen and W. Yang, *J. Am. Chem. Soc.*, 2010, **132**, 6498–6506.

30 Y. Hu, M. Huang, H. Liu, J. Miao and C. Yang, *Angew. Chem., Int. Ed.*, 2023, **62**, e202312666.

31 J. Liu, X. Yin, M. Huang, J. Miao, N. Li, Z. Huang and C. Yang, *Adv. Mater.*, 2025, **37**, 2411610.

32 C. Lee, Y. T. Lee, C. Y. Chan, C. W. Park, S. Lee, H. I. Kwon, D. Boo, Y. Tsuchiya, S. Y. Lee and C. Adachi, *Adv. Opt. Mater.*, 2025, **13**, 2402862.

33 Z. Li, Z. Li, S. Zhang, M. Liu, G. Gao, J. You and Z. Bin, *Sci. China Mater.*, 2024, **67**, 1581–1587.

34 D. Zhang, C. Zhao, Y. Zhang, X. Song, P. Wei, M. Cai and L. Duan, *ACS Appl. Mater. Interfaces*, 2017, **9**, 4769–4777.

35 T. Huang, Q. Wang, S. Xiao, D. Zhang, Y. Zhang, C. Yin, D. Yang, D. Ma, Z. Wang and L. Duan, *Angew. Chem., Int. Ed.*, 2021, **60**, 23771–23776.

36 Y. Zhang, G. Li, L. Wang, T. Huang, J. Wei, G. Meng, X. Wang, X. Zeng, D. Zhang and L. Duan, *Angew. Chem., Int. Ed.*, 2022, **61**, e202202380.

37 L. Wu, Z. Xin, D. Liu, D. Li, J. Zhang, Y. Zhou, S. Wu, T. Wang, S.-J. Su, W. Li and Z. Ge, *Adv. Mater.*, 2025, **37**, 2416224.

38 M. Quan, Z.-L. Zhu, G. Chen, J. Miao and C. Yang, *Angew. Chem., Int. Ed.*, 2025, **64**, e202512162.

39 J. Liu, X. Yin, M. Huang, J. Miao, N. Li, Z. Huang and C. Yang, *Adv. Mater.*, 2025, **37**, 2411610.

40 Z.-G. Wu, Y. Xin, C. Lu, W. Huang, H. Xu, X. Liang, X. Cao, C. Li, D. Zhang, Y. Zhang and L. Duan, *Angew. Chem., Int. Ed.*, 2024, **63**, e202318742.

41 Y.-T. Lee, C.-Y. Chan, N. Matsuno, S. Uemura, S. Oda, M. Kondo, R. W. Weerasinghe, Y. Hu, G. N. I. Lestanto, Y. Tsuchiya, Y. Li, T. Hatakeyama and C. Adachi, *Nat. Commun.*, 2024, **15**, 3174.

42 J. Liu, J. Miao, J. Dong, Z. Chen, Z. Huang and C. Yang, *Adv. Mater.*, 2025, e13987.

43 T. Fan, S. Zhu, X. Cao, X. Liang, M. Du, Y. Zhang, R. Liu, D. Zhang and L. Duan, *Angew. Chem., Int. Ed.*, 2023, **62**, e202313254.

44 G. Meng, H. Dai, Q. Wang, J. Zhou, T. Fan, X. Zeng, X. Wang, Y. Zhang, D. Yang, D. Ma, D. Zhang and L. Duan, *Nat. Commun.*, 2023, **14**, 2394.

45 L. Yuan, Z.-L. Tu, J.-W. Xu, H.-X. Ni, Z.-P. Mao, W.-Y. Xu and Y.-X. Zheng, *Sci. China:Chem.*, 2023, **66**, 2612–2620.

46 G. Meng, J. Zhou, X.-S. Han, W. Zhao, Y. Zhang, M. Li, C.-F. Chen, D. Zhang and L. Duan, *Adv. Mater.*, 2024, **36**, 2307420.

47 L. Li, Y. Xu, Y. Sun, Y. Qu, W. Cui, L. Guo, P. Zheng, Y. Wang and C. Li, *Adv. Mater.*, 2026, **38**, e11560.

48 X. Cai, J. Wei, Z. Li, Y. Pu, Y. Wu and Y. Wang, *Chem. Sci.*, 2025, **16**, 11539–11547.

49 J. Wang, D. Chen, J. M. Moreno-Naranjo, F. Zinna, L. Frédéric, D. B. Cordes, A. P. McKay, M. J. Fuchter, X. Zhang and E. Zysman-Colman, *Chem. Sci.*, 2024, **15**, 16917–16927.

50 Q. Wang, L. Yuan, C. Qu, T. Huang, X. Song, Y. Xu, Y. X. Zheng and Y. Wang, *Adv. Mater.*, 2023, **35**, 2305125.

51 Y. Yang, N. Li, J. Miao, X. Cao, A. Ying, K. Pan, X. Lv, F. Ni, Z. Huang, S. Gong and C. Yang, *Angew. Chem., Int. Ed.*, 2022, **61**, e202202227.

52 X.-J. Liao, D. Pu, L. Yuan, J. Tong, S. Xing, Z.-L. Tu, J.-L. Zuo, W.-H. Zheng and Y.-X. Zheng, *Angew. Chem., Int. Ed.*, 2023, **62**, e202217045.

53 F. Zhang, F. Rauch, A. Swain, T. B. Marder and P. Ravat, *Angew. Chem., Int. Ed.*, 2023, **62**, e202218965.

54 H. Jiang, D. Ai, J. Jin, Z. Xie and W.-Y. Wong, *Sci. China:Chem.*, 2025, **68**, 2804–2819.